Plasma heating with strong poloidal Ohmic currents

D. J. Holly, S. C. Prager, and J. C. Sprott
University of Wisconsin, Madison, Wisconsin 53706

(Received 27 July 1982; accepted 14 July 1983)

The feasibility of using strong poloidal currents to heat plasmas has been examined experimentally in Tokapole II, operating as a toroidal octupole. The plasma resistivity ranges from that of Spitzer to about 1500 times Spitzer resistivity, as predicted by mirror-enhanced resistivity theory. This allows large powers (approximately 2 MW) to be coupled to the plasma at modest current levels. However, the confinement time is reduced by the heating, apparently due to a combination of the input power location (near the walls of the vacuum tank) and fluctuation-enhanced transport.

I. INTRODUCTION

Plasma heating with poloidal currents in toroidal devices with deep magnetic mirrors, such as low-q, very-high-aspect-ratio devices (compact tori) and internal ring multipoles, may possess interesting advantages over conventional heating with toroidal currents. The large fraction of trapped particles enhances the resistivity, perhaps allowing large power deposition at modest current levels. Also, it is not known whether a current limit, analogous to the Kruskal–Shafranov limit, exists for this type of heating. We have chosen to test this hypothesis in a toroidal multipole configuration, in which very deep wells are provided by four internal rings (yielding approximately 80% trapped particles); in addition, the Ohmic currents are not necessary for plasma confinement, allowing variation of the current from zero to a large value. We are also interested in examining heating methods to push multipole plasmas to higher energies for general plasma studies[1,2] and for assessment as advanced fuel reactors.[3]

Previous researchers[4,5] have examined the effects of Ohmic currents in multipoles. The work reported in the present paper differs from this previous research in several ways:

(1) The electric fields in the present experiment range up to 150 V/m, a factor of 15 above the electric fields in previous experiments. Thus significantly larger Ohmic power is deposited in the plasma.

(2) We measure energy confinement and enhanced transport in addition to measuring the plasma resistivity.

(3) The plasma current is almost entirely poloidal in the present experiment, whereas much of the previous work involved measurement of (primarily toroidal) currents near the minor axis.

In the following we discuss, after description of the discharge characteristics in Sec. II, the resistivity enhancement, confinement degradation, and fluctuation enhancement in Secs. III, IV, and V. The discussion and conclusions are presented in Secs. VI and VII.

II. APPARATUS AND DISCHARGE CHARACTERISTICS

Tokapole II[6] is a small (major radius 50 cm, square cross section 44 cm $\times$ 44 cm) pulsed toroidal device which is normally operated as a tokamak with a four-node poloidal divertor. For these experiments, however, it was operated as a toroidal octupole. Figure 1 shows the poloidal flux plot for this mode of operation. The mirror ratio on a flux surface ranges from about 2 to infinity (on the separatrix with no toroidal field). Near the outer wall, where most of the plasma current flows, this ratio ranges from 3 to 8 as the toroidal field is varied. A significant fraction of the electrons is thus trapped in the magnetic mirrors and cannot contribute to the plasma current; this enhances the resistivity (Sec. III).

The field timing is shown in Fig. 2. The poloidal magnetic field (typically 1 kG at the outer wall midplane) is crowbarred at its peak, and the toroidal magnetic field is then pulsed. The resulting poloidal electric field drives plasma currents of typically 20 kA, producing plasmas with $n_e \sim 5\times 10^{12}$ cm^{-3} and $T_e \sim 30$ eV.

The poloidal plasma current is determined by measuring the change it produces in the toroidal field, using a small movable magnetic probe. The toroidal winding current is monitored with a Rogowski coil; the poloidal plasma current and current density are then obtained from

$$I_p = (2\pi R/\mu_0)\Delta B_T - \Delta I_w,$$

where R is the distance to the major axis, Δ refers to the change produced by the plasma current, I_w is the equivalent one-turn toroidal winding current, and I_p is the total poloi-

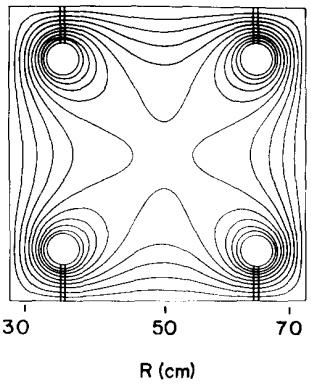

FIG. 1. Poloidal flux plot of Tokapole II operated as an octupole.

 0031-9171/83/113435-05$01.90

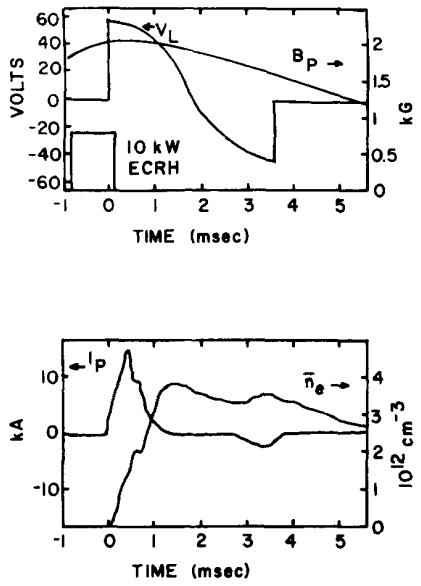

FIG. 2. Time evolution of a typical poloidal Ohmic heating shot, showing poloidal loop voltage V_L; poloidal magnetic field B_P; poloidal plasma current I_P; and line-averaged electron density $\bar{n}_e$.

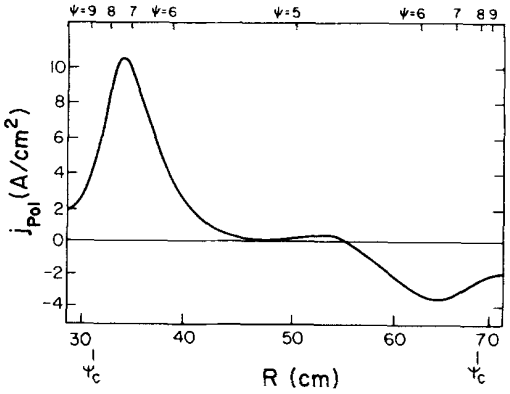

FIG. 4. Typical poloidal plasma current density obtained with a movable magnetic field probe as a function of radius on the midplane. The difference between the inside and outside current density peaks is due mainly to the $1/R$ dependence of the magnetic field geometry. Also shown are the flux surfaces Ψ and the critical flux surface Ψ_c.

dal plasma current between the probe and the wall of the vacuum tank. The calculated vacuum electric field (Fig. 3) peaks near the wall, giving a current density which peaks slightly inside of Ψ_c, the critical flux surface outside of which the plasma is magnetohydrodynamic (MHD) unstable (Fig. 4).

The plasma density is monitored by a 70 GHz microwave interferometer and movable Langmuir probes. Initially the density peaks near the walls, then moves inward to peak on the separatrix late in time (Fig. 5). Fluctuations in the density are very large ($\delta n/n \sim 100\%$) in the region where the current flows. The fluctuation magnitude is independent of the direction of the density gradient. The fluctuations are low frequency ($f < 10$ kHz) and persist for the duration of the Ohmic current.

III. RESISTIVITY

The resistivity of the plasma for current flow parallel to field lines, averaged around a poloidal flux surface, is given by[5]

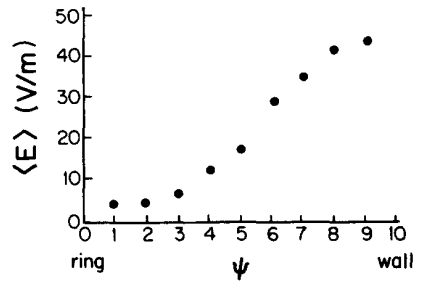

FIG. 3. Calculated poloidal electric field averaged around a flux surface as a function of flux surface Ψ. The flux surfaces correspond to those shown in Fig. 1, with $\Psi = 0$ at the ring surface and $\Psi = 10$ at the wall.

$$\langle \eta \rangle = \left(\frac{B}{J}\right)\frac{V_{\|}}{\oint (B^2/B_P)dl},$$

where B_P is the poloidal magnetic field, $V_{\|}$ is the poloidal loop voltage around the flux surface, and J and B are the plasma current density and total magnetic field, respectively, at the point of measurement. This equation allows the flux-surface-averaged resistivity to be determined by a measurement of J and B at any point on the flux surface.

The resistivity measured in this way ranges from about the Spitzer value to roughly 1500 times Spitzer as collisionality varies from highly collisional to collisionless (Fig. 6).

Previous researchers[5,6] have developed a simple theory, based upon heuristic arguments, to evaluate the effects of the multipole magnetic mirrors on plasma resistivity. The theory gives the resistivity scaling and magnitude in three regimes as the collisionality is varied. For high collisionality, Coulomb collisions are the dominant process; interactions with the magnetic mirrors are relatively infrequent, and the resistivity is simply Spitzer[7] resistivity. For very low collisionality, only the fraction of electrons which is not trapped in the magnetic mirrors can carry a current; when these electrons become mirror trapped as a result of small-angle scattering they immediately cease to contribute to the current. In the intermediate collisionality regime, again only the untrapped fraction of electrons can contribute to the current, but after an electron is trapped in the magnetic mirrors, it continues to contribute to the current until it bounces a relatively long time $\tau \sim 1/\nu_b$ later, with ν_b the bounce frequency for an electron in the magnetic mirrors.

The predictions of this theory in the three regimes of collisionality are shown as the solid lines in Fig. 6. The two solid lines in the intermediate and low collisionality regimes represent the effects of electric field detrapping for the range of electric fields used in these experiments. The data fit well in the intermediate regime, but the resistivity continues to rise in the collisionless regime. This is in agreement with previous multipole Ohmic heating results.

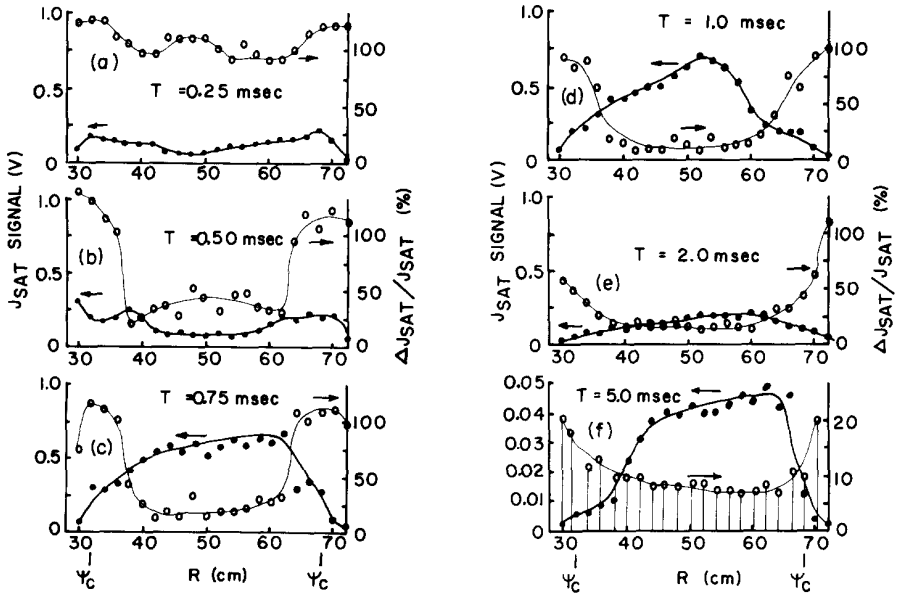

FIG. 5. Ion saturation current J_{sat} and its fluctuation level $\Delta J_{sat}/J_{sat}$ as a function of radius on the midplane, for various times during a poloidal Ohmic discharge. Note the expanded scale and error bars in (f). Also shown is the critical flux surface Ψ_c.

Thus the multipole magnetic mirrors appear to enhance the resistivity above the Spitzer value as expected in the intermediate collisionality regime, but the resistivity enhancement continues to rise at very low collisionality.

IV. CONFINEMENT

The enhanced resistivity allows large power deposition (up to approximately 2 MW in these experiments) at modest current levels; however, the heating seriously degrades the confinement. The electron temperature remains below 30 eV, giving an energy confinement time $\tau_E \lesssim 30\,\mu$sec (Fig. 7). Measurements of vacuum ultraviolet radiation show far too little radiated energy to account for the input power. After the heating is turned off, the plasma density decays with a time constant ~ 1 msec, corresponding to a diffusion coefficient $D \sim 350 \times D_{\text{classical}} \sim 0.1 \times D_{\text{Bohm}}$. The poor confinement during the heating is ascribed to two causes. The Ohmic power is peaked near the wall of the vacuum tank, giving a much shorter distance across which the energy must diffuse to escape to the walls than if the energy were peaked on the separatrix as in a standard octupole configuration. A one-dimensional energy transport code[8] indicates that this should lead to confinement degradation by a factor of 4 to 10 over a standard octupole configuration.

In addition, the fluctuations enhance the particle transport. Measurements of local electric field and local density fluctuations (δn and δE) with a small three-tipped probe yield a particle flux $\Gamma = \langle \delta n \delta E_\perp / B \rangle$ (where $E_\perp$ is the local electric field perpendicular to the local magnetic field **B**). Typical waveforms of $\delta E_\perp$ and δn measured in this way are shown in Fig. 8. Note that the phase shift between the two signals is approximately 180 deg, indicating a net particle flux directed outward (toward the wall of the vacuum tank). Averaging the fluctuations over the duration of the Ohmic heating pulse yields a transport velocity $\langle v \rangle$ on the order of 3×10^5 cm/sec. Since a typical distance from the location of

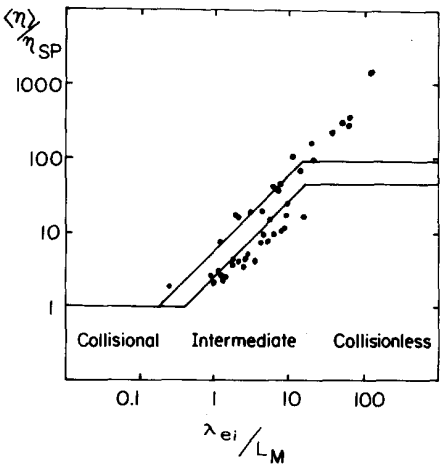

FIG. 6. Resistivity enhancement over Spitzer resistivity as a function of plasma collisionality. Here λ_{ei} is the distance an electron travels in an electron–ion effective 90° scattering time; L_m is the distance along magnetic field lines between field maxima.

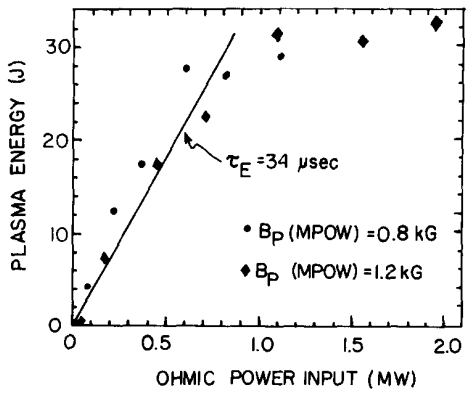

FIG. 7. Plasma energy $E = 1.5\, N_e k T_e$ as a function of Ohmic input power coupled to the plasma, for two poloidal field values.

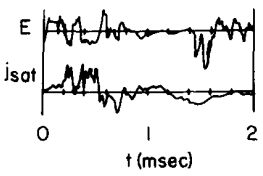

FIG. 8. Local electric field perpendicular to B and local ion saturation current fluctuations measured with a small three-tipped Langmuir probe. The saturation current signal has been passed through a 1 kHz, 6 dB/octave high-pass filter; the peak-to-peak saturation current fluctuation is approximately 100% of the average value of the saturation current. The peak electric field shown is about 8 V/cm. After about 1 msec, the field line pitch is so great that the $\delta E_{\parallel}$ shown is no longer approximately perpendicular to B.

peak heating current to the wall is 5 cm, this indicates a confinement time of about 20 μsec, consistent with the observed energy confinement time. The overall particle confinement time indicates a diffusion coefficient during the heating of $\sim 7500\, D_{\text{classical}} \sim 2D_{\text{Bohm}}$. Measurements during the heating do not show a simple scaling of the diffusion coefficient with plasma and magnetic field parameters, however.

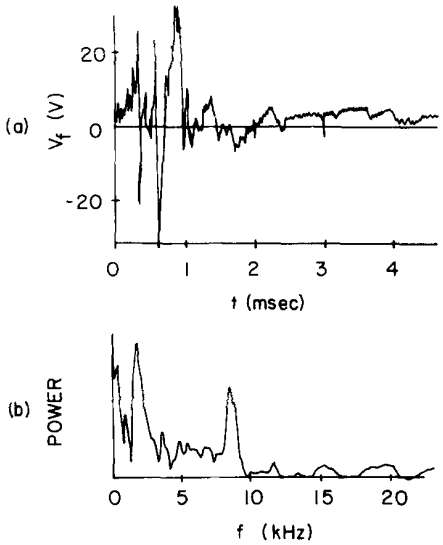

FIG. 9. A typical fluctuation signal and power spectrum. (a) Typical floating potential signal as a function of time at $R = 67$ cm on the midplane. (b) Typical power spectrum of floating potential signal.

V. FLUCTUATIONS

Fluctuations persist at very high levels during the heating, even at low heating currents. Initially the density peaks outside the separatrix, then moves in to peak on the separatrix later in time. Thus one might expect a pressure-driven instability in the early stages of the discharge. In fact, however, the fluctuation level does not depend on the direction of the density gradient: ion saturation fluctuation levels are always on the order of 100% in the region where the Ohmic current flows, even when the density is peaked on the separatrix. The fluctuation amplitude is large even well inside Ψ_{crit}.

A typical fluctuation signal and power spectrum are shown in Fig. 9. There is usually a broad frequency peak between $f = 5$ and $f = 10$ kHz. Excluding this peak, the overall power spectrum has roughly a f^{-a} form, where $0.7 < a < 1.5$. There is very little fluctuation activity at frequencies $f > 10$ kHz.

Fluctuation wavelength measurements were made in several cases where the 5 to 10 kHz peak was strong. The measurement is complicated by the fact that the field line pitch changes significantly ($\sim 20\%$) during a fluctuation period. The floating potential was measured with two probes, one fixed and the other moved to each of several locations. The phase shift between the two signals as a function of time and probe location was combined with the calculated field line pitch as a function of time to yield wavelengths parallel to and perpendicular to the magnetic field. Calculations for the case shown in Fig. 9 and a few similar cases yield $\lambda_{\perp} \sim 20$ cm, $\lambda_{\parallel} > 120$ cm. The correlation between the two probe signals was poor when the probes were spaced more than about 110 cm apart toroidally.

Due to the mirror trapping, the fraction of electrons which is available to carry the plasma current is typically only a few tenths; this gives rise to the desired resistivity enhancement but also implies a high electron streaming velocity u_d. The ratio u_d/v_{eth} (v_{eth} is the electron thermal speed) ranges from 0.2 to 50 in these experiments, compared to 0.01 in a typical tokamak. These high streaming speeds are favorable for exciting current-driven instabilities. Because most of the plasma density is produced by the poloidal heating, the ratio u_d/v_{eth} actually decreases with increasing poloidal loop voltage.

The high streaming speed of the current-carrying electrons might be expected to excite a high-frequency two-stream instability. Such high-frequency radiation might be expected to be much less deleterious to confinement than the large-amplitude, low-frequency fluctuations described above. Nevertheless, we performed a cursory search for radiation in the range of frequencies near the electron plasma frequency using a diode detector with a horn antenna. The apparatus was capable of detecting signals, which, if isotropically radiated, correspond to ~ 3 W ($\sim 10^{-6}$ of the Ohmic input power) radiated from the entire plasma. With similar apparatus previous researchers[9] have been able to observe microwave emission from plasmas subjected to high electric fields. However, we did not observe any high-frequency radiation. Langmuir probes with frequency response extending to tens of MHz have detected no plasma activity in the frequency range near the ion cyclotron frequency, typically a few MHz in these plasmas.

A computer program[10] which solves the Grad–Shafranov equation in octupole flux coordinates indicates that the plasma current does not upset the octupole equilibrium; the flux surfaces are almost identical with and without plasma current. The rotational transform due to the plasma current is small compared to the vacuum transform; this suggests that (similar to the stellarator case[11]) the fluctuations are probably not due to an ideal current-driven MHD instability.

The wavelength and frequency measurements indicate a phase propagation velocity perpendicular to **B** approximately the same as v_*, the electron diamagnetic drift velocity, with propagation in the electron diamagnetic drift direction. This is consistent with both drift waves and resistive

MHD modes. In order to couple energy from the streaming electrons, the drift wave would need a nonzero parallel wave vector component $\mathbf{k}\cdot\mathbf{B}\neq 0$, while the resistive MHD modes must have a resonant layer where $\mathbf{k}\cdot\mathbf{B} = 0$; however, the $\mathbf{k}\cdot\mathbf{B}$ required for current-driven drift waves is small enough so that either instability is consistent with the measured $\lambda_\parallel > 120$ cm. Calculated growth times for the resistive MHD modes are much less than the fluctuation period. Conditions for both types of instability are thus satisfied in these plasmas, and it is difficult to distinguish one from the other.

VI. DISCUSSION

The rising resistivity in the collisionless regime is believed due to scattering of electrons from fluctuations. Mirror-dominated resistivity theory[6] predicts a transition from the intermediate collisionality regime to the collisionless regime when $\nu_b > \nu_{1c}$, where ν_{1c} is the frequency at which current-carrying electrons become trapped in the magnetic mirrors. If electron–ion collisions are the dominant scattering process then ν_{1c} is proportional to ν_{ei}, the effective 90 deg electron–ion collision frequency; this gives rise to the "knee" in the theoretical resistivity shown on the right side of Fig. 6.

However, if another scattering process exists (such as electrons scattering from fluctuations) it may become the dominant scattering process as ν_{ei} is reduced, and may prevent ν_{1c} from decreasing as the electron–ion collisionality is reduced. Thus the resistivity would continue to follow the intermediate regime scaling (where the electron mean free path is almost independent of plasma parameters) even at very low electron–ion collisionalities. Data taken by Brouchous[12] in which the plasma underwent both a noisy and a quiet phase supports the speculation that the rising resistivity in the collisionless regime is due to fluctuations. During the noisy phase the collisionless resistivity was enhanced above the theoretical value as in Fig. 6; during the quiet phase the collisionless resistivity was in good agreement with the theoretical prediction. During poloidal Ohmic heating, the fluctuation level is always high. A computer code is currently being developed by Brouchous to quantitatively account for the effect of the fluctuations on resistivity in the collisionless regime.

Since the fluctuation magnitude is independent of the direction of the density gradient and since the electron streaming speed is so high in these experiments, it seems probable that the fluctuations are current driven. Provision of an initial plasma to relieve the Ohmic electric field of start-up responsibility may allow suppression of these instabilities. A Marshall gun source currently being added to the machine may provide sufficient initial density to allow observation of the onset of the instabilities.

VII. CONCLUSION

Poloidal Ohmic heating does allow large powers to be coupled to the plasma at modest current densities due to the mirror-enhanced resistivity; however, the confinement is seriously degraded. This is believed due to a combination of the input power location near the wall, which degrades the confinement by a factor of 4 to 10; and enhanced transport due to fluctuations, which further reduces the confinement by a factor of 2 to 5. However, the loss enhancement due to the input power location remains an unattractive feature of this heating scheme.

ACKNOWLEDGMENTS

The authors thank R. Dexter and N. Brickhouse for providing measurements of impurity radiation and optical measurements of electron temperature. H. Garner and M. Phillips provided computer programs used in this research. We acknowledge helpful discussions with T. Osborne, J. Callen, and D. Brouchous. The assistance of T. Lovell, R. Vallem, and their technical crew is appreciated.

Portions of this paper were based on the Ph.D. thesis of D. Holly (University of Wisconsin, 1982).

This work was supported by the United States Department of Energy.

3. C. Prager, Nucl. Inst. Methods **207**, 187 (1983).
[2]R. N. Dexter, C. M. Fortgang, S. C. Prager, J. C. Sprott, E. J. Strait, and J. C. Twichell, in *Proceedings of the Third Varenna-Grenoble International Conference on Heating in Toroidal Plasmas* (Commission of the European Communities, Brussels, 1982), Vol. 1, p. 333.
[3]J. Dawson, Bull. Am. Phys. Soc. **24**, 42 (1979).
[4]D. E. Lencioni, Phys. Fluids **14**, 566 (1971).
[5]D. Brouchous and J. Etzweiler, Phys. Fluids **23**, 2557 (1980).
[6]A. P. Biddle, R. N. Dexter, R. J. Groebner, D. J. Holly, B. Lipschultz, M. W. Phillips, S. C. Prager, and J. C. Sprott, Nucl. Fusion **19**, 1509 (1979).
[7]L. Spitzer and R. Harm, Phys. Rev. **89**, 977 (1953).
[8]H. R. Garner, Bull. Am. Phys. Soc. **25**, 967 (1980).
[9]B. A. Demidov, N. I. Elagin, D. D. Ryutov, and S. D. Fanchenko, Sov. Phys. JETP **21**, 302 (1965).
[10]M. W. Phillips, B. Lipschultz, T. Osborne, K. Miller, S. C. Prager, and J. C. Sprott, Bull. Am. Phys. Soc. **23**, 900 (1978).
[11]K. Miyamoto, Nucl. Fusion **18**, 87 (1978).
[12]D. A. Brouchous (private communication).